Penerbit Akademia Baru

Journal of Advanced Research in Fluid Mechanics and Thermal Sciences

Journal homepage: www.akademiabaru.com/arfmts.html
ISSN: 2289-7879

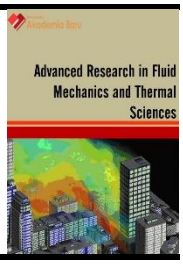

Conservative and Oscillationless Semi-Lagrangian Schemes for Tsunami Modelling

Open Access

Wei Chek Moon[1], Tze Liang Lau[1], How Tion Puay[2,*]

[1] School of Civil Engineering, Engineering Campus, Universiti Sains Malaysia, 14300 Nibong Tebal, Penang, Malaysia
[2] River Engineering and Urban Drainage Research Centre (REDAC), Engineering Campus, Universiti Sains Malaysia, 14300 Nibong Tebal, Penang, Malaysia

ARTICLE INFO

Article history:
Received 7 October 2019
Received in revised form 29 October 2019
Accepted 31 October 2019
Available online 30 November 2019

ABSTRACT

In this paper, we applied and evaluated the performance of a higher-order scheme based on volume/surface integrated average based multi-moment method (VSIAM3) for the simulation of tsunami propagation on land. The advection term in the momentum equation was solved by using the conservative semi-Lagrangian scheme with third-order accuracy based on constrained interpolation profile (CIP–CSL3). In order to reduce the numerical diffusion and suppress the numerical oscillation, we adopted the Collela-Woodward (CW) reconstruction method to approximate the slope in the CIP–CSL3 interpolation function. The moving interface between air-water was captured by using the volume of fluid (VOF) method. We opted for the algebraic type of VOF to avoid geometrical surface reconstruction difficulty, where the tangent of hyperbola for interface capturing (THINC) scheme was used to compute a sharp and smear-less air-water interface. We first compared the validity and stability of our two-dimensional numerical model by conducting a numerical test with dam-break flow problem. Results were excellent in terms of the front propagation speed (3% slower than physical experiment). Our numerical model was then applied to simulate tsunami propagation on land and the results were compared to the hydraulic experimental results as well as the numerical results of a proprietary software (FLOW-3D). The results demonstrated an improvement of the flow surface resolution and a better wave arrival prediction as compared to the FLOW-3D model. The accuracy of maximum pressure estimation was also improved by as much as 5% through the upgrade of the original first-order gradient approximation to the higher-order CW method in the CIP-CSL3 interpolation.

Keywords:
VSIAM3; CIP-CSL3_CW; VOF; tsunami-induced pressure

1. Introduction

Numerical two-phase models for incompressible viscous fluid are widely used for the simulation of tsunami propagation on land [1-3]. Due to violent flow and large surface deformation, tsunami simulation has remained a fastidious concern for coastal engineers and researchers. The accuracy of

* *Corresponding author.*
E-mail address: redac_puay@usm.my (How Tion Puay)

the model in reproducing accurate wave propagation speed and impact force upon impact on a vertical wall is critical in tsunami mitigation planning.

As the flow is undergoing impulsive motion and drastic changes in pressure both temporally and spatially, the accuracy of the numerical solution is highly dependent on the performance of the momentum equation solver. In order to handle such non-linearity, an ideal solver must avoid implicit artificial viscosity [4] and be conservative to correctly capture shock wave motion [5]. The volume/surface integrated average based multi-moment method (VSIAM3) introduced by Xiao *et al.,* [6] provides numerical solver which is oscillationless and conservative. The VSIAM3 framework inherited the conservative property of the finite volume method (FVM) as the governing equations are cast in conservative form.

The conservative property is further enhanced due to a utilization of the volume integrated average (VIA) and the surface integrated average (SIA) of physical flow variables in the conservative advection transport solver for the momentum equation, known as the CIP-CSL scheme [5]. The order of the CIP-CSL scheme depends on the choice of the interpolation polynomial. When a third-order polynomial is constructed over a cell by utilizing the VIA and SIA, the advection transport scheme is referred to as the CIP-CSL3 scheme [7]. Besides having the advantage from the conservative constraints, the CIP-CSL3 provides access to the gradient parameter used in the interpolation function which acts as an explicit artificial parameter to suppress numerical diffusion.

Besides the first-order gradient approximation in the original CIP-CSL3 scheme, there are different order accurate approximations proposed by Xiao and Yabe [8], namely the CIP-CSL3_UNO, CIP-CSL3_CWMM and CIP-CSL3_HYMAN schemes, each adopting the Uniform Non-oscillatory (UNO), Collela-Woodward with minmod limiter (CWMM) and Hyman (HYMAN) gradient approximation, respectively. Each approximation has its own superiority in terms of the diffusive and oscillatory errors. Figure 1 presents the transportation of a square wave using the above-mentioned schemes with constant velocity. Although the CIP-CSL3_CWMM scheme effectively avoids the numerical oscillation at the sharp step, the sharpness of the solution is sacrificed.

It is worth to highlight that the CIP-CSL3_CWSB scheme (CW with superbee limiter) could retain the sharpness of the solution better than the CIP-CSL3_CWMM scheme (Figure 1). Therefore, in this study, we propose the superbee (SB) limiter to replace the minmod limiter (MM) which is originally devised in the Collela-Woodward (CW) reconstruction method. The resulting CIP-CSL3_CWSB scheme is then used for sine wave advection with conditions similar to Li *et al.,* [9]. Table 1 shows the numerical results of L_1 and L_{max} errors in sine wave propagation at t = 1 s. Based on Table 1, the L_{max} order is improved, indicating that the CIP-CSL3_CWSB scheme could handle discontinuity slightly better than the original CW which uses a kind of minmod limiter. However, the CIP-CSL3_CWSB scheme still maintains at second-order accuracy for L_1 due to the use of slope limiter.

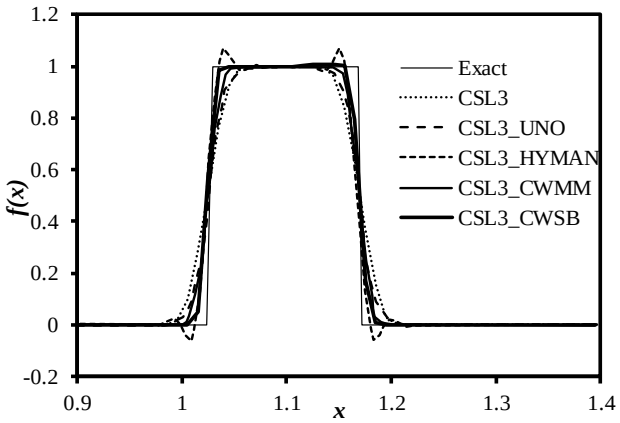

Fig. 1. A transported square wave after 1000 step calculations (CFL = 0.2)

Table 1
L_1 and L_{max} errors in sine wave propagation at t = 1 s

CIP-CSL3_CWSB					CIP-CSL3_CWMM (Results adopted from Li *et al.,* [9])				
No. of grid (N)	L_1 error	L_1 order	L_{max} error	L_{max} order	No. of grid (N)	L_1 error	L_1 order	L_{max} error	L_{max} order
100	6.19×10^{-4}	-	5.83×10^{-3}	-	100	5.85×10^{-4}	-	5.04×10^{-3}	-
200	1.39×10^{-4}	2.15	2.00×10^{-3}	1.54	200	1.18×10^{-4}	2.31	1.80×10^{-3}	1.49
400	3.01×10^{-5}	2.21	6.78×10^{-4}	1.56	400	2.29×10^{-5}	2.36	6.27×10^{-4}	1.52
800	6.21×10^{-6}	2.28	2.27×10^{-4}	1.58	800	4.57×10^{-6}	2.33	2.14×10^{-4}	1.55

It is also worth to note that the temporary moment (TM) algorithm by Yokoi *et al.,* [10] is adopted in this study to reduce the numerical viscosity in the original VSIAM3 method. Apart from high accuracy governing equation solver, the interface tracking method also determines the overall performance of the numerical model for the study purpose. The algebraic-type volume of fluid (VOF) method over the geometrical-type VOF (such as PLIC) is employed to avoid the complicated geometrical surface reconstruction. The VOF function is solved with the Tangent of Hyperbola for Interface Capturing (THINC) scheme [11], which is a highly diffusion-less advection scheme based on the hyperbolic interpolation profile.

In view of afore-mentioned challenges in simulating the tsunami wave propagation and its impulsive motion during impact on a vertical wall, the study entails bringing and merging superior solver and interface tracking scheme for the development of a highly accurate and efficient numerical model. In this study, a multiphase model with highly efficient solver is developed based on the VSIAM3 framework with CIP-CSL3_CWSB advection transport solver and a smear-less and oscillation-less interface capturing THINC scheme. The developed numerical model is first verified with the typical dam-break-flow benchmarking test, followed by a model validation of tsunami propagation on land.

2. Numerical Procedure

2.1 Governing Equations

The conservative form of momentum equation and continuity equation for an incompressible flow (Navier-Stokes equations) are as follows

$$\frac{\partial}{\partial t}\int_{\Omega} \mathbf{u}\, dV + \int_{\Gamma} \mathbf{u}(\mathbf{u}\cdot\mathbf{n}) dS = \frac{1}{\rho}\int_{\Gamma} -P\mathbf{n} + \boldsymbol{\tau}\cdot\mathbf{n}\, dS + \int_{\Omega} \mathbf{g}\, dV \quad (1)$$

$$\int_{\Gamma} \mathbf{u} \cdot \mathbf{n}\, dS = 0 \tag{2}$$

where $\mathbf{u}$ and $\mathbf{g}$ respectively denote the velocity and gravitational acceleration vectors, $\mathbf{n}$ is the normal vector on the surface Γ of the control volume Ω, P is the pressure, ρ is the fluid density, t is the time and $\boldsymbol{\tau}$ is the stress tensor. In our numerical model, $\boldsymbol{\tau}$ includes the viscous and turbulence stress tensor, where the Large Eddy Simulation (LES) turbulence model [12] is adopted. In the LES turbulence model, the eddy viscosity is modelled by using the Wall-Adapting Local Eddy-viscosity (WALE) model [13].

2.2 Framework of VSIAM3 for 2D Model

In the two-dimensional VSIAM3 framework, the VIA and SIA degenerate to the surface integrated average (SIA) and the line integrated average (LIA), respectively. The SIA and LIA are defined as in Figure 2, based on the M-grid [14] system where the pressure is defined at the cell center, whereas the velocities are defined at the cell center and on the cell boundaries as well. For brevity, the definition of SIA and LIA for velocity in x-direction only is given here

$$u_{ij}^{SIA} = \frac{1}{\Delta x \Delta y} \int_{i-1/2}^{i+1/2} \int_{j-1/2}^{j+1/2} u(x,y)\ dydx \tag{3}$$

$$u_{i-1/2,j}^{LIA} = \frac{1}{\Delta y} \int_{j-1/2}^{j+1/2} u\left(x_{i-1/2}, y\right) dy \tag{4}$$

$$u_{i,j-1/2}^{LIA} = \frac{1}{\Delta x} \int_{i-1/2}^{i+1/2} u\left(x, y_{j-1/2}\right) dx \tag{5}$$

The SIA and LIA of the velocities and pressure are used for the calculation in the VSIAM3 procedure. It is worth to mention that the SIA and LIA of the velocities will be used to establish the CIP-CSL3_CWSB interpolation profile.

2.3 Numerical Algorithm

In the VSIAM3 method, time integration of Eq. (1) is performed by the fractional step method [15], by which the calculation of the equation is divided into the advection phase and non-advection phase as follows,

Step 1: Advection phase: $\mathbf{u}^n \rightarrow \mathbf{u}^*$,

Solving $\frac{\partial}{\partial t} \int_{\Omega} \mathbf{u}\, dV + \int_{\Gamma} \mathbf{u}(\mathbf{u} \cdot \mathbf{n}) dS = 0$

Step 2: Non-advection phase 1: $\mathbf{u}^* \rightarrow \mathbf{u}^{**}$,

Solving $\frac{\partial}{\partial t} \int_{\Omega} \mathbf{u}\, dV = \frac{1}{\rho} \int_{\Gamma} \boldsymbol{\tau} \cdot \mathbf{n}\ dS + \int_{\Omega} \mathbf{g}\, dV$

Step 3: Non-advection phase 2: $\mathbf{u}^{**} \rightarrow \mathbf{u}^{n+1}$,

Solving $\frac{\partial}{\partial t}\int_{\Omega} \mathbf{u}\, dV = \frac{1}{\rho}\int_{\Gamma} P\mathbf{n}\, dS$

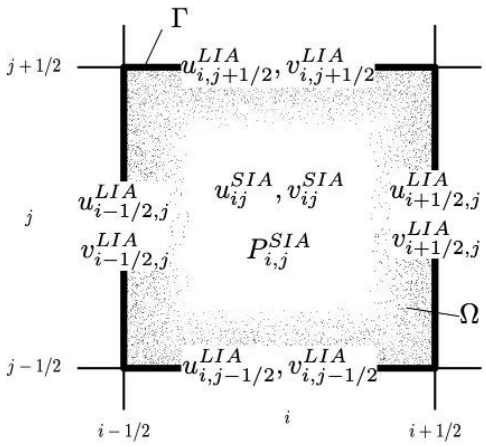

Fig. 2. M-Grid system

In Step 1, the velocity is upgraded to an intermediate value (denoted by a superscript '*') after solving the advection terms with the initially known velocity field at time step *n*. Next, the shear stress is evaluated by using **u*** to advance the previously computed velocity field. Prior to Step 3, pressure iteration starts, where the pressure field for the new time step (*n*+1) is evaluated based on **u**** as computed in Step 2. More details on the algorithm using the fractional step method can be further obtained in Moon *et al.,* [16]. In this study, the advection phase is solved using the CIP-CSL3_CWSB scheme. Reference for the CW interpolation and SB limiter is available in Collela and Woodward [17] and Roe [18], respectively.

Since the CIP-CSL3_CWSB scheme is a 1-D solver which only updates quantity in the control volume based on the flux on the surface normal to the flow direction, other surface average quantities in the remaining directions are updated by the directional splitting method [19]. In the original VSIAM3, the Time Evolution Converting (TEC) algorithm is used to update the non-normal components. For example, when CIP-CSL3_CWSB is used to perform *Step 1* for the advection transport in x-direction for u (velocity component in x-direction), the LIA value $u^{n,LIA}_{i-1/2,j}$ is updated to $u^{*,LIA}_{i-1/2,j}$. With TEC, the non-normal component $u^{n,LIA}_{i,j-1/2}$ is updated as follows,

$$u^{*,LIA}_{i,j-1/2} = u^{n,LIA}_{i,j-1/2} + \frac{1}{2}\left(u^{*,SIA}_{i,j} - u^{n,SIA}_{i,j} + u^{*,SIA}_{i,j-1} - u^{n,SIA}_{i,j-1}\right) \quad (6)$$

where $u^{*,SIA}_{i,j}$ and $u^{n,SIA}_{i,j}$ are the SIA values after and before CIP-CSL3_CWSB calculation, respectively. However, the TEC tends to introduce implicit artificial viscosity for some low Reynold's number cases.

In this study, TM method is used to update these non-normal components, where TM method is based on the fact that the 1-D CIP-CSL schemes (and its variants) can be used to advect any properties in one particular direction at a time. In the two-dimensional case, the SIA+LIA values are used in the advection transport of the LIA property, while the one-dimensional case would involve the LIA and PV (point value). Therefore, in order to advect the non-normal component (for example $q^{n,LIA}_{i,j-1/2}$) with CIP-CSL scheme, the non-normal component is treated as the LIA and its corresponding PVs are calculated by averaging the neighbouring LIAs. The PVs are referred to as the "temporary" moments, as they act as auxiliary variables during the advection transport calculation. For example, when the advection transport for non-normal component $u^{n,LIA}_{i,j-1/2}$ is performed with CIP-CSL scheme, the TM

at point $(i-1/2, j-1/2)$ and $(i+1/2, j-1/2)$ are needed, as shown in Figure 3. The TM at point $(i-1/2, j-1/2)$ is evaluated as follows,

$$u_{i-1/2,j-1/2}^{n,TM} = \frac{1}{2}(u_{i,j-\frac{1}{2}}^{n,LIA} + u_{i-1,j-1/2}^{n,LIA}) \tag{7}$$

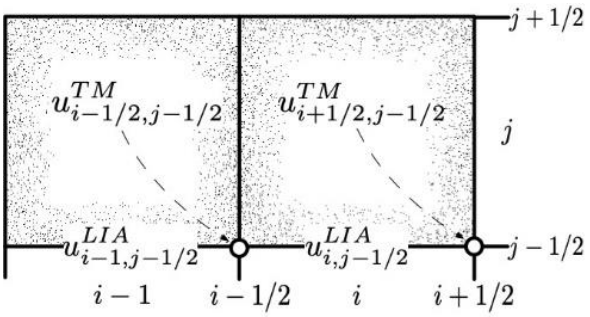

Fig. 3. Schematic diagram of the definition of temporary moments which are needed when advecting the non-normal component $u_{i,j-1/2}^{n,LIA}$ with CIP-CSL in *x*-direction

2.4 Interface Capturing

In the numerical model, the interface between the fluids (air and water) is represented by the algebraic-type VOF method. Upon obtaining the latest divergence free velocity field, VOF function *f* is advected according to the advection equation as follows,

$$\frac{\partial}{\partial t}\int_\Omega f\, dV + \int_\Gamma (\mathbf{u}f)\cdot \mathbf{n} dS - \int_\Omega f(\nabla\cdot\mathbf{u}) dV = 0 \tag{8}$$

The advection equation in Eq. (8) is discretized by using FVM. Instead of using the Heaviside step function in the original VOF method as proposed by Hirt and Nicolas [20], the diffusionless THINC scheme by Xiao *et al.,* [11] is used to evaluate the fluxes (second term in Eq. (8)) by employing the hyperbolic tangent function $F_i(x)$ as shown in Eq. (9). A constant steepness parameter β of 3.5 is used in the numerical model to keep the sharpness of the interface.

$$F_i(x) = \frac{\alpha}{2}\left\{1+\gamma\tanh\left[\beta\left(\frac{x-x_{i-1/2}}{\Delta x_i}-\tilde{x}_i\right)\right]\right\} \tag{9}$$

3. Model Verification

3.1 Numerical Setup

In this section, the numerical model (CIP-CSL3_CWSB) is verified against the benchmark testing case by Lobovsky *et al.,* [21]. A numerical domain of 1610 mm x 600 mm is set with initial conditions similar to the physical experiment by Lobovsky *et al.,* [21]. Non-slip condition is set for the side wall and floor, while an outlet condition is applied for the ceiling. A 10 mm grid size is used in the domain for both *x* and *y* directions.

3.2 Free Surface Profile

Figure 4 depicts the flow profiles at different times of the numerical simulation compared with the experimental results by Lobovsky *et al.,* [21]. In Figure 4, the contour lines with density functions of 0.10, 0.15, 0.20 and 0.25 are used to indicate the numerical results of the free surface profile.

As shown in Figure 4(a), a rectangular water column (dotted line) of 300 mm (H_o) x 600 mm (L_o) is initially confined between the walls and a gate. The advancing downstream wave front is observed upon the removal of the dam gate at t = 0.16 s (Figure 4(a)). At this stage, the CIP-CSL3_CWSB model exhibits the capability of reproducing almost identical flow as in the physical experiment. At around t = 0.45 s, the wave hits the downstream wall and climbs up the downstream wall, forming a thin film attached to the wall (Figure 4(b)). Subsequently at t = 0.86 s, the rising water begins to collapse. A similar phenomenon is observed for the numerical simulation during the overturning and breaking of the free surface (Figure 4(c)). The results qualitatively confirm the good performance of the numerical model in reproducing accurate flow, not only at the initial stage but also during turbulent stage at around t = 1.17 s (Figure 4(d)).

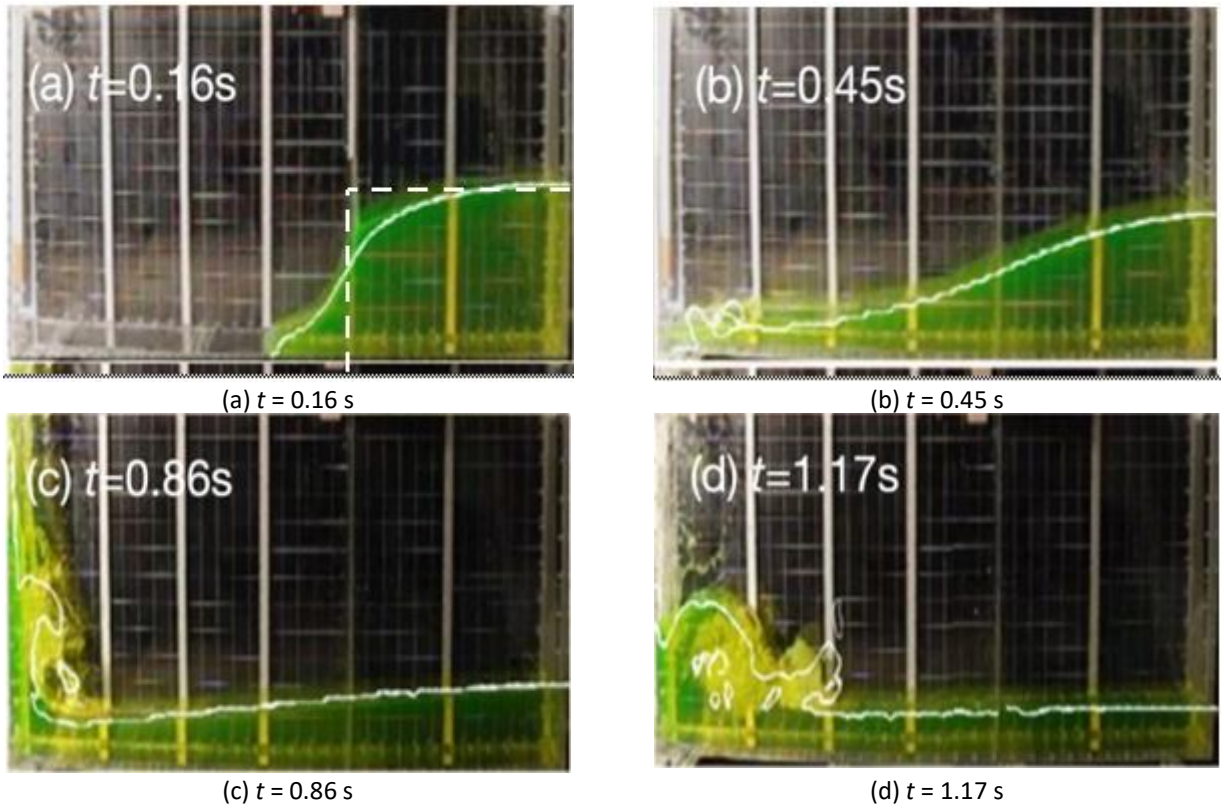

(a) t = 0.16 s (b) t = 0.45 s

(c) t = 0.86 s (d) t = 1.17 s

Fig. 4. Comparison of free surface profile between experimental results (Lobovsky *et al.,* [21]) and numerical results (contour line)

3.3 Front Wave Propagation

For quantitative assessment, the variation of the dimensionless front wave propagation (L/H_o) between the numerical and experimental data is shown in Figure 5. The results in figure shows that the numerical model performs excellently with the simulated front wave propagation is only 3% slower as compared to the experimental results. Overall, there is a good agreement in terms of the free surface profile and front wave propagation between the simulation and experimental results.

Figure 6 shows the residual history for the continuity equation. Based on Figure 6, the maximum residual is around 1 x 10^{-4} within 2 s of simulation, which shows satisfactory convergence for the incompressible flow.

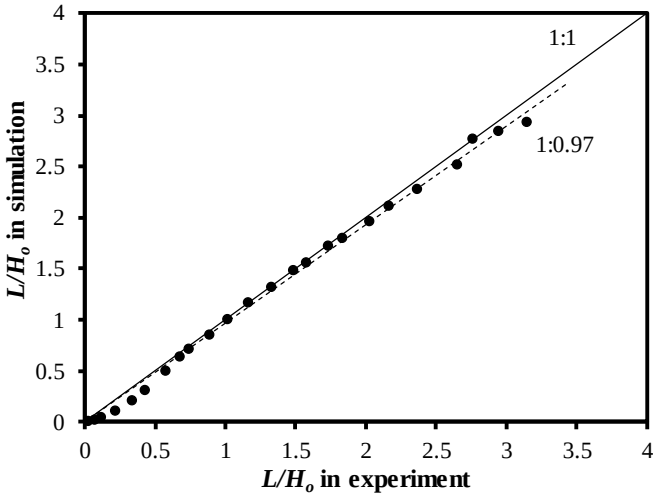

Fig. 5. Variation of front wave propagation between experimental and numerical results

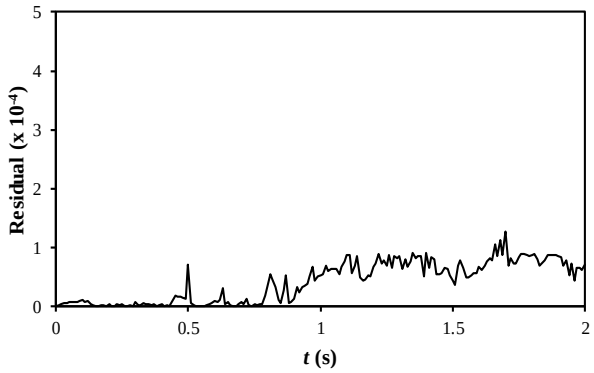

Fig. 6. Residual history for continuity equation

4. Model Validation

4.1 Experimental Setup

A 1:50 scaled hydraulic experiment was conducted in a 40 m long, 1 m wide and 1 m deep wave flume, at the Hydraulic Laboratory in Universiti Sains Malaysia. Figure 7 illustrates the laboratory setup for the tsunami propagation on land. A continuous plane slope of 1:200 and 1:125 is constructed to represent the typical coast profile in Malaysia. A still water depth of 470 mm in the flume represents the offshore region. The bed of the shore is assumed to be rigid. For simplicity, the shore bed friction is neglected. More details on the laboratory setup can be found in Moon *et al.,* [22].

In this study, the tsunami impact on a slab-on-grade building subjected to a 40 mm nominal wave height is investigated. An 8 m (W) x 12 m (L) x 3.6 m (H) model is used to represent a typical single-storey residential building in Malaysia. The building block model is made from the acrylic plates to ensure its rigidity. In the hydraulic experiment, the building model is positioned at the horizontal dry bed section (at a horizontal distance of 3.225 m and a vertical height of 25 mm from the shoreline) as shown in Figure 7.

4.2 Numerical Setup

For validation purpose, a partial flume length domain is considered in the numerical simulation as shown in Figure 8. A 40 mm nominal wave condition is generated by using the time histories of wave height (H2) and flow velocity (V2) at the shoreline obtained from the hydraulic experiment. These values are set as the inlet boundary condition. Non-slip condition is set for the floor, whereas an outlet condition is set for the ceiling and right-hand side wall. The 1:125 sloping bed and the building model are set using the Fractional Area/Volume Obstacle Representation (FAVOR) technique [23]. A variable grid system is applied, where grid sizes of 10 and 5 mm are used in the domain for *x* and *y* directions, respectively. The time steps in the simulations for all the cases tested are 1.0 x 10^{-4} s, therefore the average Courant number in the domain is kept below 0.1 in the computation.

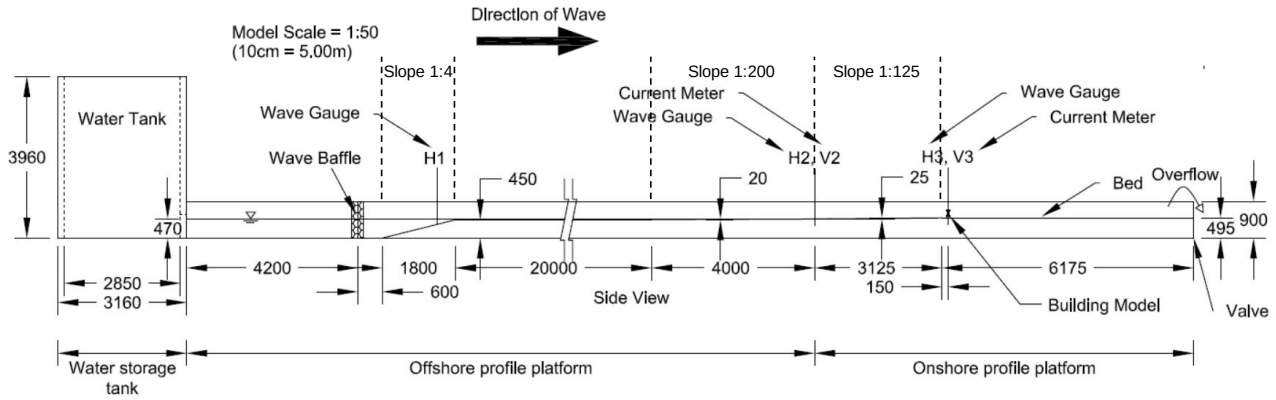

Fig. 7. Schematic diagram of laboratory setup (dimensions are in mm)

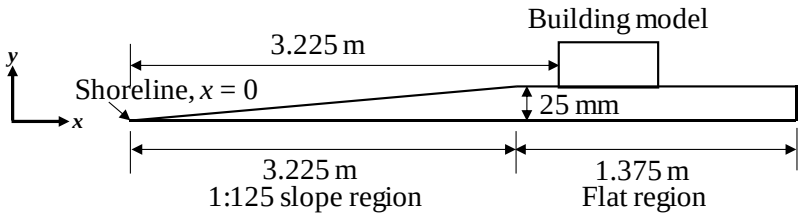

Fig. 8. Numerical model setup (not to scale)

4.3 Free Flow Condition (Without Building Model)

The measured and simulated wave height and flow velocity at the onshore region (H3 and V3) are compared in Figures 9(a) and 9(b), respectively. The measured and simulated data are indicated by solid and dotted lines, respectively. The results from FLOW-3D (a proprietary software) which is using the first-order scheme are included. It allows the comparison of the performance of the numerical model with different order of the numerical schemes.

Based on Figure 9(a), the arrival time of the wave at H3 is at around t = 2.2 s for the experimental case, whereas the simulated wave arrives 0.1 s later for the CIP-CSL3_CWSB model and more than 0.4 s later for the FLOW-3D model. This shows the superiority of the CIP-CSL3_CWSB model in reproducing an accurate flow velocity on dry shore. Based on Figures 9(a) and 9(b), the simulation results are in reasonable agreement with the experimental data in terms of the maximum height and velocity of the wave. However, the simulated flow velocity by both CIP-CSL3_CWSB and FLOW-3D models at the later stage (t > 4 s) appears to be slightly higher than the measured one. Based on the results in Figures 9(a) and 9(b), turbulent flow is observed with Reynolds number (Re) ranging from

27057 to 36780. The maximum flow velocity is approximately 1.5 m/s with Mach number (Ma) of 0.001 at a room temperature of 20°, which justifies the incompressible flow (Ma < 0.3).

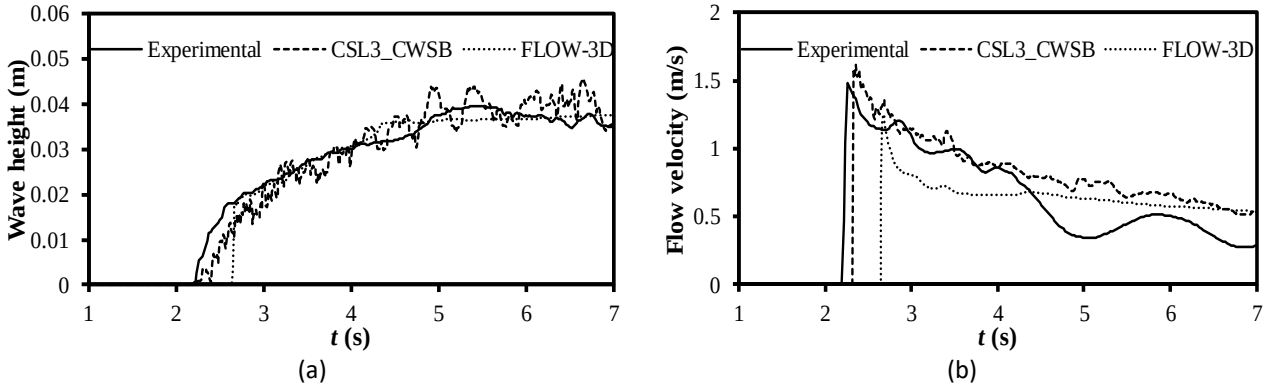

Fig. 9. Comparison of (a) height and (b) velocity of incoming wave

4.4 Wave Attack on Building Model

Figure 10 shows the snapshots of wave impacting the building model (marked as dotted lines), taken from the side of the wave flume. In the following discussion, the time t = 0 s denotes the time when the wave first hits the building model. Based on Figure 10, the free surface configurations are reasonably reproduced by the CIP-CSL3_CWSB model, although the piled-up wave is slightly higher than that in the hydraulic experiment.

The height of the building model (72 mm) is greater than the 40 mm nominal wave condition. Consequently, only some amount of water is found landing on top of the building model after the piled-up wave collapses at t = 0.5 s, as shown in Figure 10(a). Such flow configuration is observed in the results of the CIP-CSL3_CWSB model (Figure 10(b)). On the other hand, the wave overtopping effect on the building model is not obvious in the results of the FLOW-3D model (Figure 10(c)).

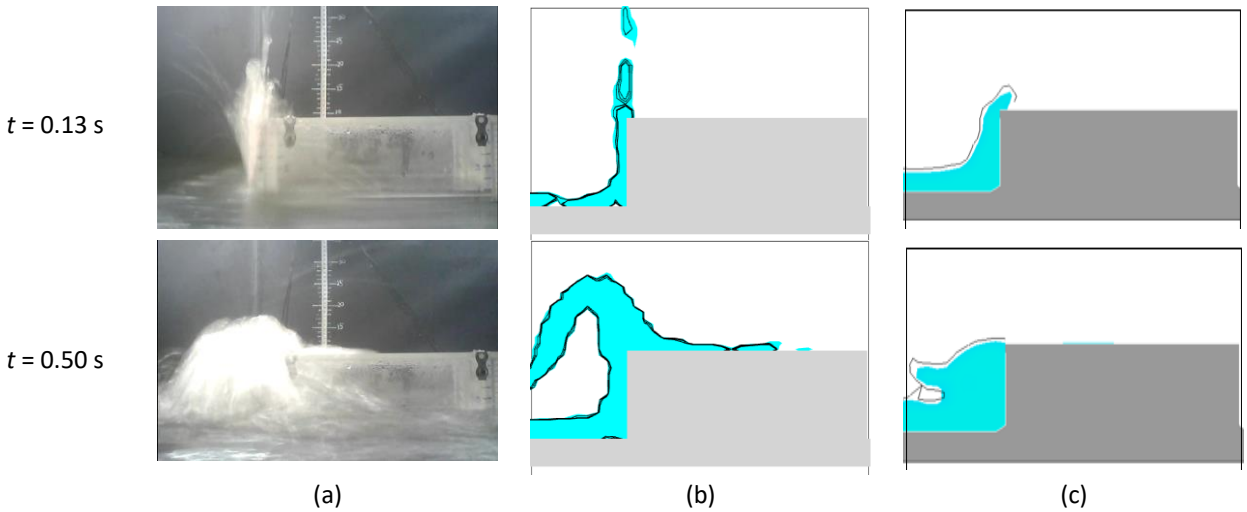

Fig. 10. Sequences of wave attack on building model in (a) experiment, (b) simulation by CIP-CSL3_CWSB model and (c) simulation by FLOW-3D model

4.5 Wave Pressure on Building Model

In the hydraulic experiment, the tsunami-induced loading on the front face of the building model is quantified by using the diaphragm type pressure gauges with the diameter of 10 mm and thickness of 3 mm, placed from bottom to top at a distance of 21 mm along the front face centreline of the building model. Figure 11 displays the representative pressure time histories recorded on the building model.

Maximum pressures are observed at the front face bottom-most part of the building model in the hydraulic experiment right after the impingement of the leading edge on the building model. Thus, only the bottom-most pressure gauge (P1) reading is discussed here. In the hydraulic experiment, the maximum pressure head of P1 is recorded to be about 10 cm (Figure 11). The peak pressure at P1 is satisfactorily reproduced in both numerical models.

After the piled-up wave collapsed, the wave starts to reflect from the building model and interferes with the incoming waves. This explains that the pressure drops and fluctuates right after the peak pressure as shown in Figure 11. Subsequently, the front face pressure enters a sustained phase as the main body of the tsunami wave impinges the building model. It is apparent from Figure 11 that the CIP-CSL3_CWSB model slightly overestimates the front face pressure on the building model, especially during the sustained phase. This may be due to the inability of a two-dimensional numerical model to simulate the lateral motion of the waves at this phase.

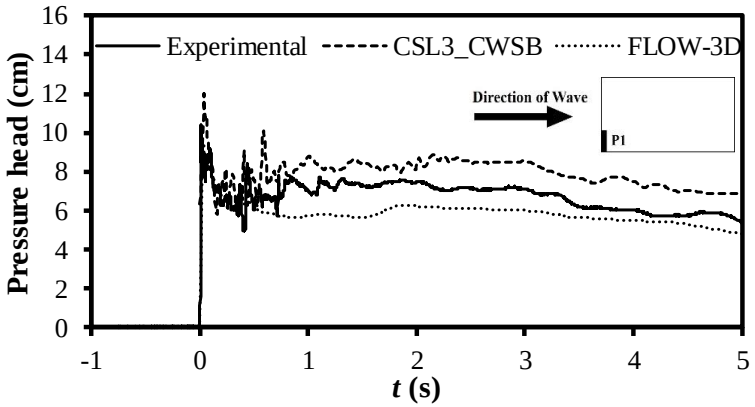

Fig. 11. Comparison of measured and simulated pressure time histories

Figure 12 depicts the variation of the front face maximum pressure for the numerical models. The results by using the original CIP-CSL3 scheme with the first-order gradient approximation are also included. Based on Figure 12, the FLOW-3D model with the first-order scheme underestimates the front face maximum pressure by around 21 %, whereas the CIP-CSL3_CWSB model could accurately predict the wave-induced loading on the building model, although there is a slight overestimation of about 5%. The accuracy of the maximum pressure estimation improves as much as 5 % for the CIP-CSL3_CWSB model (using higher-order gradient approximation) as compared to the original CIP-CSL3 (using first-order gradient approximation).

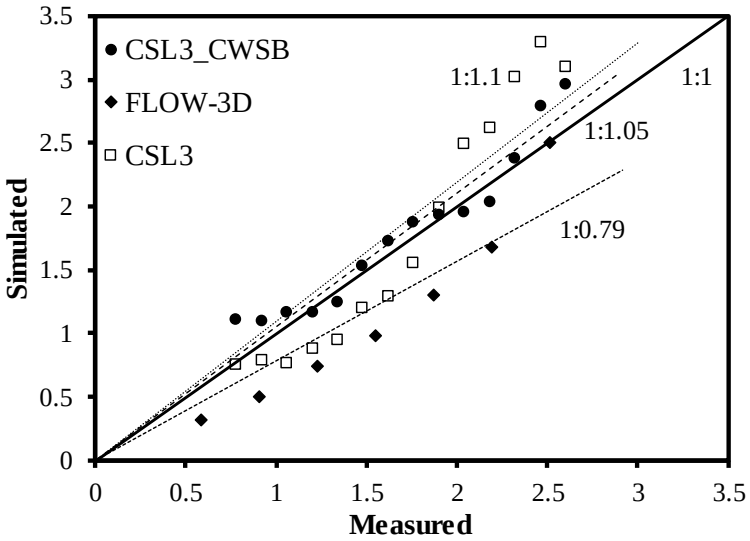

Fig. 12. Variation of maximum front face pressure between experimental and numerical results

5. Conclusions

In this study, the performance and robustness of a conservative and oscillationless semi-Lagrangian scheme in the simulation of tsunami propagation on land were investigated. The results demonstrated that with fine-tuning of the original scheme, the new CIP-CSL3_CWSB model could deliver higher accuracy in terms of the reproduction of tsunami propagation speed and peak pressure. The numerical model also reproduced the complicated surface configuration during and after the wave impingement on the obstacle satisfactorily. Therefore, the numerical model showed promising performance for future coastal hydrodynamics applications.

Acknowledgement

The experimental facilities were supported by the Ministry of Science, Technology and Innovation (MOSTI), Malaysia through ScienceFund Research Grant (04-01-05-SF0562) and JICA Project for AUN/SEED-Net through Collaborative Research for Alumni (CRA) 2013. The authors also acknowledge the financial support provided by the School of Civil Engineering, Universiti Sains Malaysia.

References

[1] Xiao Hong and Wenrui Huang. "Numerical modeling of wave runup and forces on an idealized beachfront house." *Ocean Engineering* 35, no. 1 (2008): 106-116.

[2] Inoue, S. and Y. Mizushima. "Simulation of three dimensional tsunami inundation into the inside of building." *Proceeding of The 10th International Conference on Urban Earthquake Engineering* (2013): 1909-1912.

[3] Cho Minsang, Sungwon Shin, Hyun-Doug Yoon, and Daniel T. Cox. "Numerical simulation of tsunami force acting on vertical walls." *Journal of Coastal Research* 79 (2017): 289-293.

[4] Borthwick, A. "Comparison between two finite-difference schemes for computing the flow around a cylinder." *International Journal for Numerical Methods in Fluids* 6, no. 5 (1986): 275-290.

[5] Takashi Yabe, Ryotaro Tanaka, Takashi Nakamura, and Feng Xiao. "An exactly conservative semi-lagrangian scheme (CIP-CSL) in one dimension." *Monthly Weather Review* 129, no. 2 (2001): 332-334.

[6] Feng Xiao, Akio Ikebata, and Takashi Hasegawa. "Numerical simulations of free-interface fluids by a multi-integrated moment method." *Computers & structures* 83, no. 6-7 (2005): 409-423.

[7] Feng Xiao, and Akio Ikebata. "An efficient method for capturing free boundaries in multi-fluid simulations." *International Journal for Numerical Methods in Fluids* 42, no. 2 (2003): 187-210.

[8] Feng Xiao, and Takashi Yabe. "Completely conservative and oscillationless semi-lagrangian schemes for advection transportation." *Journal of Computational Physics* 170, no. 2 (2001): 498-522.

[9] Li Qijie, Syazana Omar, Xi Deng, and Kensuke Yokoi. "Constrained interpolation profile conservative semi-Lagrangian scheme based on third-order polynomial functions and essentially non-oscillatory (CIP-CSL3ENO) scheme." *Communications in Computational Physics* 22, no. 3 (2017): 765-788.
[10] Yokoi Kensuke, Mikito Furuichi, and Mikio Sakai. "An efficient multi-dimensional implementation of VSIAM3 and its applications to free surface flows." *Physics of Fluids* 29, no. 12 (2017): 121611(1-31).
[11] Xiao, F., Y. Honma, and T. Kono. "A simple algebraic interface capturing scheme using hyperbolic tangent function." *International Journal for Numerical Methods in Fluids* 48, no. 9 (2005): 1023-1040.
[12] Schumann, U. "Direct and large eddy simulation of turbulence. Summary of the state of art 1987." In *In Von Karman Inst. for Fluid Dynamics, Introduction to the Modeling of Turbulence 83 p (SEE N88-15972 08-34)*. 1987.
[13] Nicoud Frank, and Frédéric Ducros. "Subgrid-scale stress modelling based on the square of the velocity gradient tensor." *Flow, Turbulence and Combustion* 62, no. 3 (1999): 183-200.
[14] Xiao, F., X. D. Peng, and X. S. Shen. "A finite-volume grid using multimoments for geostrophic adjustments." *Monthly Weather Review* 134, no. 9 (2006): 2515-2526.
[15] Kim John, and Parviz Moin. "Application of a fractional-step method to incompressible Navier-Stokes equations." *Journal of computational physics* 59, no. 2 (1985): 308-323.
[16] Moon, W. C., H. T. Puay, and T. L. Lau. "Numerical simulation of free surface flow using a multiphase model with higher order scheme." In *AIP Conference Proceedings*, vol. 2020, no. 1, p. 020078. AIP Publishing, 2018.
[17] Collela Philip, and Paul R. Woodward. "The piecewise parabolic method (PPM) for gas-dynamical simulations." *Journal of Computational Physics* 54, no. 1 (1984): 174-201.
[18] Philip L. Roe. "Characteristic-based schemes for the Euler equations." *Annual review of fluid mechanics* 18, no. 1 (1986): 337-365.
[19] Takashi Nakamura, Ryotaro Tanaka, Takashi Yabe, and Kenji Takizawa. "Exactly conservative semi-Lagrangian scheme for multi-dimensional hyperbolic equations with directional splitting technique." *Journal of Computational Physics* 174, no. 1 (2001): 171-207.
[20] Cyril W., Hirt, and Billy D. Nichols. "Volume of fluid (VOF) method for the dynamics of free boundaries." *Journal of computational physics* 39, no. 1 (1981): 201-225.
[21] Libor Lobovský, Elkin Botia-Vera, Filippo Castellana, Jordi Mas-Soler, and Antonio Souto-Iglesias. "Experimental investigation of dynamic pressure loads during dam break." *Journal of Fluids and Structures* 48 (2014): 407-434.
[22] Moon, Wei Chek, Lerk Qing Chiew, Kah Win Cheong, Yi Cong Tee, Jan Bong Chun, and Tze Liang Lau. "An experimental study for estimating tsunami wave forces acting on building with seaward and landward macroroughness." *Ocean Engineering* 186 (2019): 106116.
[23] Hirt, C. W., and J. M. Sicilian. "A porosity technique for the definition of obstacles in rectangular cell meshes." In *International Conference on Numerical Ship Hydrodynamics, 4th*. 1985.